Published in IET Generation, Transmission & Distribution
Received on 14th October 2007
Revised on 17th June 2008
doi: 10.1049/iet-gtd:20080285

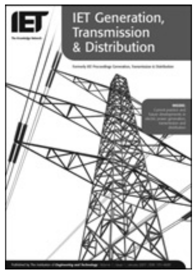

ISSN 1751-8687

Differential equation-based fault locator for unified power flow controller-based transmission line using synchronised phasor measurements

S.R. Samantaray[1] *L.N. Tripathy*[2] *P.K. Dash*[2]

[1]*Department of Electrical Engineering, National Institute of Technology, Rourkela, India*
[2]*Department of Electrical and Electronics Engineering, Silicon Institute of Technology, Bhubaneswar, India*
E-mail: sbh_samant@yahoo.co.in

Abstract: The fault location algorithm based on a differential equation-based approach for a transmission line employing a unified power flow controller (UPFC) using synchronised phasor measurements is presented. First, a detailed model of the UPFC and its control is proposed and then, it is integrated into the transmission system for accurately simulating fault transients. The method includes the identification of fault section for a transmission line with a UPFC using a wavelet-fuzzy discriminator. Features are extracted using a wavelet transform and the normalised features are fed to the fuzzy logic systems for the identification of fault section. After the identification of the fault section, the control shifts to the differential equation-based fault locator that estimates the fault location in terms of the line inductance up to the fault point from the relaying end. Shunt faults are simulated with wide variations in operating conditions and a pre-fault parameter setting. The instantaneous fault current and voltage samples at the sending and receiving ends are fed to the designed algorithm sample by sample, which results in the fault location in terms of the line inductance. The proposed method is tested for different fault situations with wide variations in operating conditions in the presence of a UPFC.

1 Introduction

In the current open access environment, transmission systems are being required to provide increased bulk power transfer capability and to accommodate a much wider range of possible generation patterns. This has led to an increased focus on transmission constraints and on the means by which much constraint can be alleviated. FACTS [1] devices offer a versatile alternative to conventional reinforcement methods. One of the more intriguing and potentially most versatile classes of FACTS devices is the unified power flow controller (UPFC) [2]. These devices, which consist of two linked self-commutating converters, connected to AC systems through series and shunt transformers, offer a unique combination of fast shunt and series compensation. The UPFC offers new horizons in terms of power system control, with the potential to independently control up to three power system parameters, for instance bus voltage, line active power and line reactive power. Although the use of a UPFC improves the power transfer capability and stability of a power system, certain other problems emerge in the field of power system protection, in particular transmission line protection [3–5].

The presence of a fault with a FACTS device in the fault loop affects both transient and steady-state components of the voltage and current. Therefore the calculations of the apparent impedance (which includes the line inductance) for fault location from the relaying end should take into account the variable series voltage source and its angle, and the shunt current and admittance presented by the shunt converter of the UPFC. However, if the UPFC is not present in the fault loop, the calculations of the apparent impedance are similar to that of the ordinary transmission lines. Further, depending on the severity and the type of fault and its duration, the magnitude and phase angle of the variable series voltage source are adjusted. Thus, because of the presence of UPFC in a transmission system, the calculation of the fault location is greatly affected and difficult to deal with.

Some research has been done to evaluate the performance of the distance relay for a transmission system with FACTS controllers. The determination of the fault location using an Adaptive Kalman filter [6] for advanced series compensation (ASC) line employs differences in transient current signals for faults including and not including ASC. It provides the fault location in terms of line resistance and reactance. However, the Kalman-filtering approach finds its limitation in that fault resistance cannot be modelled and further it requires a number of different filters to accomplish the task. In another approach [7], the apparent impedance is calculated and it is found that the trip boundaries are significantly affected in the presence of a UPFC in the transmission line. Thus, finding the fault location from the relaying point in the presence of the UPFC is a challenging issue to deal with. The research work done earlier does not include a pre-fault parameter setting, whereas the proposed study includes the same, which has a larger impact on fault analysis in a power system.

This paper presents a new approach for fault location using differential equation-based approach [8] using synchronised phasor measurements. The proposed scheme works on the assumption that the fault detection and classification has been done. The pre-fault and post-fault boundary are detected by using the fault detector that uses a short data window (four samples) algorithm [9]. The final indication of the fault is given only when three consecutive comparisons give the difference more than a specified threshold value. There are two parts in the proposed method. The first part identifies the fault section showing whether the fault includes a UPFC or not, using a wavelet-fuzzy discriminator. After the fault section is identified, the fault locator determines the fault location. The fault location algorithm works on the assumption that the voltage and current signals of both the sending and receiving ends are synchronised. Two fault locators are designed, one for a fault before the UPFC (not including UPFC) and the other for a fault after the UPFC (including UPFC). After knowing the occurrence of the fault, before or after the UPFC, the corresponding differential equation-based fault locator starts calculating the distance of the fault from the relaying point in terms of the line inductance. The proposed study includes setting the UPFC and transmission line parameters resultant from the pre-fault power flow solutions, which are not included in the earlier studies [3–5]. The pre-fault magnitude and phase angle of the series injected voltage plays a vital role in the functionality of the UPFC. The proposed method is tested for different faults with wide variations in operating conditions.

2 UPFC and transmission system model

2.1 Transmission line employing UPFC

The schematic diagram for the studied system is shown in Fig. 1*a*. The system is simulated using a PSCAD (EMTDC) package as shown in the Fig. 1*b*. The network has two areas connected by the transmission line of 400 kV. The transmission line is of a distributed model with zero sequence impedance $Z_0 = 96.45 + j335.26\ \Omega$ and positive sequence impedance $Z_1 = 9.78 + j127.23\ \Omega$ and $E_1 = 400$ kV and $E_2 = 400 \angle \delta$ kV. Z_{S1} and Z_{S2} are the source impedances of the sending- and receiving-end sources, respectively. Z_{L1} is the line impedance from the relaying point to the UPFC location and Z_{L2} is the line impedance from the UPFC location to the receiving end. The UPFC is connected at the mid point of the transmission line.

The basic components of the UPFC are two voltage source inverters (VSIs) sharing a common DC storage capacitor, and connected to the system through coupling transformers. One VSI is connected in shunt to the transmission system via a shunt transformer, whereas the other one is connected in series through a series transformer. The UPFC consists of two 48-pulse VSIs that are connected through a 2000 μF common DC capacitance. The STATCOM is connected to the power system through a 400/20 kV shunt transformer and injects reactive power to the transmission system to regulate the voltage at the connecting point. Another inverter SSSC connects into the power system through a 20/60 kV series transformer to inject almost sinusoidal voltage of variable magnitude and phase angle to regulate the power flow through the transmission line. A basic UPFC functional scheme is shown in Fig. 1*b*.

The relaying point is as shown in the Fig. 1*a* where data are retrieved for different fault conditions. The synchronised faulted voltage and current signals of both the sending and receiving end are retrieved and fed to the proposed differential equation-based fault location algorithms. The sampling rate is 1.0 kHz at a base frequency of 50 Hz. The UPFC is placed at 50% (mid point) of the line with series injected voltage varying from 0 to 15%. The proposed distance relaying scheme is shown in Fig. 2.

2.2 UPFC control

The UPFC control system is divided into two parts, STATCOM control and SSSC control. The STATCOM is controlled to operate the VSI for reactive power generation at the connecting point voltage V_{ref}. The voltages at the connecting points are sent to the phase-locked-loop (PLL) to calculate the reference angle, which is synchronised to the reference phase voltage. The currents are decomposed into the direct and quadrature

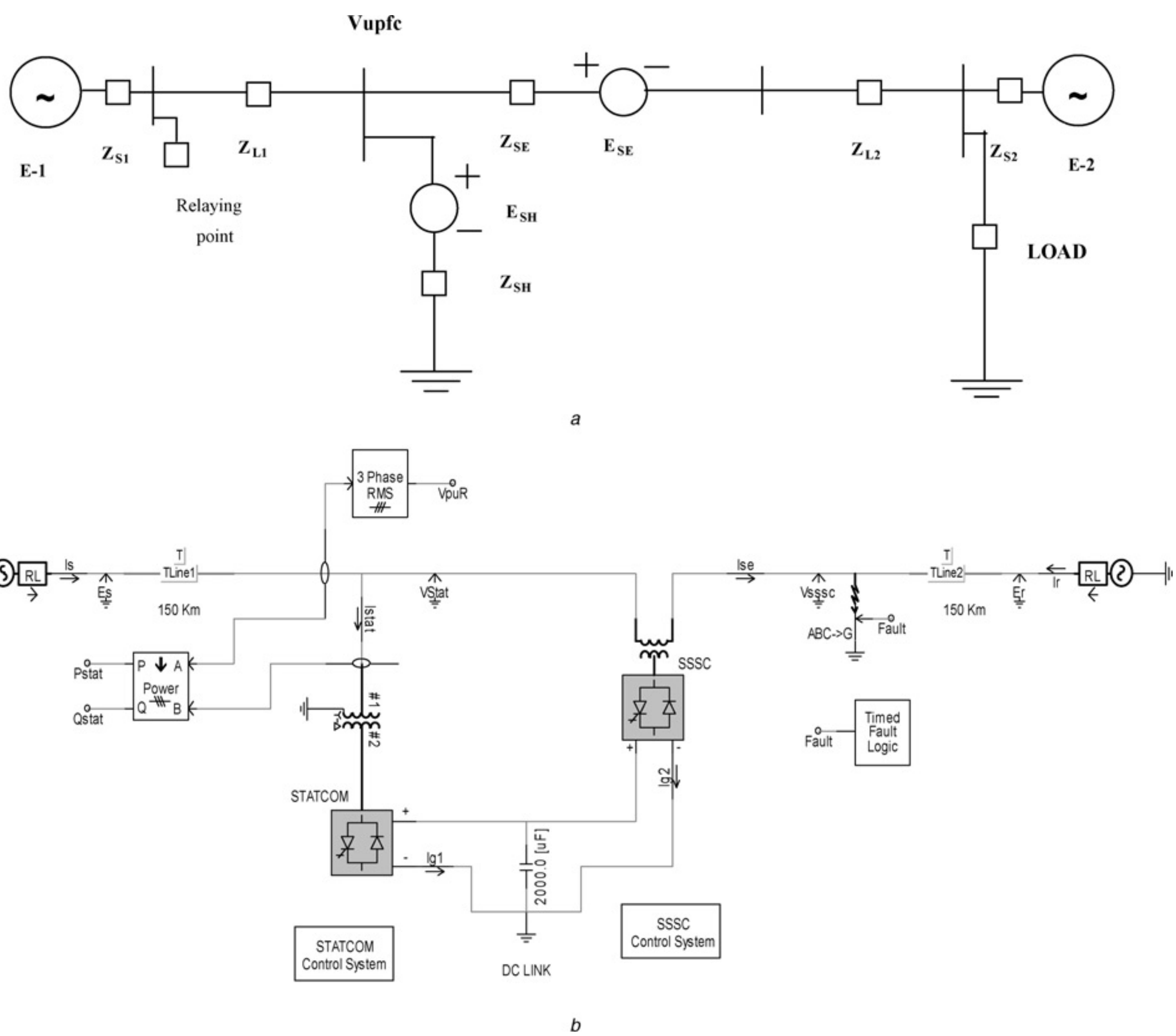

Figure 1 *UPFC based transmission system*

a Transmission system with UPFC
b UPFC-based transmission line model developed using PSCAD

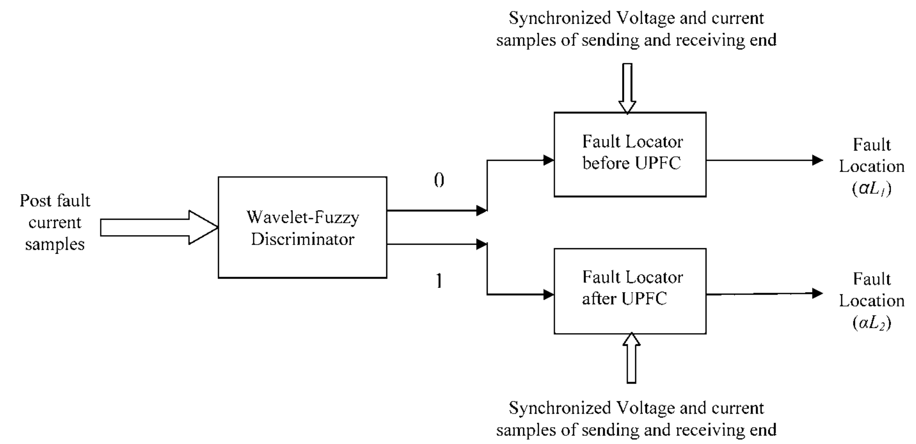

Figure 2 *Proposed protection scheme*

components, I_d and I_q by a *d*-*q* transformation using the PLL angle as reference. The magnitude of the positive sequence component of the connecting point voltage is compared with $V_{\rm ref}$ and the error is passed through the PI controller to generate $I_{\rm qref}$. The reactive part of the shunt current is compared with $I_{\rm qref}$ and the error is passed through the PI controller to obtain the relative phase angle of the inverter voltage with respect to the reference phase voltage. This

doi: 10.1049/iet-gtd:20080285

phase angle and the PLL signal are fed to the STATCOM firing circuit to generate the desired pulse for the VSI.

The series injected voltage is determined by the closed-loop control system to ensure that the desired active and reactive power flow occurs despite power system changes. The desired P_{ref} and Q_{ref} are compared with the measured active and reactive power flow in the transmission line, and the error is passed through the PI controller to derive the direct and quadrature components of the series inverter voltage, V_{dref} and V_{qref}. Thus, the series injected voltage and phase angle can be found out from the rectangular to polar conversion of the V_{dref} and V_{qref}. The dead angle (found out from the inverter voltage and DC link voltage), phase angle and the PLL signal are fed to the firing circuit to generate the desired pulse for the SSSC VSI.

3 Fault section identification

3.1 Feature extraction using wavelet transform

For fault section identification, the fault current (half cycle post-fault current) is processed through wavelet transform (db4) [10–12] and features such as x_1 and x_2 are found out from wavelet coefficients. As wavelet transform is an ideal tool for fault transient analysis and, thus, feature extraction is done by pre-processing the current signal through wavelet transform. The db4 is selected as it is well suited for power system transient analysis. The signal is decomposed into three levels of decomposition. This results in a_1 (0–250 Hz) and d_1 (250–500 Hz) in level 1, a_2 (0–125 Hz) and d_2 (125–250 Hz) in level 2, and a_3 (0–62.5 Hz) and d_3 (62.5–125 Hz) in level 3. Thus, d_1 contains fifth (250 Hz) and seventh (350 Hz) harmonic components, whereas d_2 contains third (150 Hz) and fifth (250 Hz) harmonic components, respectively. The features are extracted using the above wavelet coefficients as follows

$$x_1 = \frac{\text{energy of the detailed coefficients } (d_2)}{\text{energy of the approximate coefficients } (a_3)}$$

$$x_2 = \frac{\text{energy of the detailed coefficients } (d_1)}{\text{energy of the approximate coefficients } (a_3)}$$

Thus, x_1 and x_2 show the harmonic component information with respect to fundamental components. As in the case of a transmission line with FACTS devices such as a UPFC, higher harmonic components such as the third, fifth and seventh are highly pronounced and, thus, for section identification these above features are extracted for a final classification using fuzzy logic system (FLS).

The respective values of x_1 and x_2 are normalised and fed to the FLS to obtain the fault section. Table 1 shows values of x_1 and x_2 for different types of fault situations such as 'a–g', 'a–b', 'ab–g', 'abc' and 'abc–g' faults occurring before and after the UPFC. For an 'a–g' fault at 45% of the line, the values of x_1 and x_2 are 0.168 and 0.231, respectively. However, for a similar fault occurring at 55% of the line, the respective values are 0.814 and 0.795. Similar observations are made for an 'a–b' fault occurring before and after the UPFC. It is seen that the values of x_1 and x_2 are higher for faults after the UPFC compared to those for faults before the UPFC.

Table 1 Features x_1 and x_2 for faults at different locations

Fault location	x_1	x_2
10% (a–g at R_f = 20 Ω, α = 30°)	0.214	0.302
20% (a–g at R_f = 30 Ω, α = 45°)	0.198	0.258
45% (a–g at R_f = 50 Ω, α = 60°)	0.168	0.231
45% (a–g at R_f = 100 Ω, α = 60°)	0.112	0.168
55% (a–g at R_f = 20 Ω, α = 90°)	0.814	0.795
65% (b–g at R_f = 50 Ω, α = 30°)	0.715	0.723
90% (a–g at R_f = 20 Ω, α = 45°)	0.698	0.645
90% (a–g at R_f = 150 Ω, α = 45°)	0.625	0.612
10% (a–b at R_f = 20 Ω, α = 60°)	0.285	0.298
20% (b–c at R_f = 50 Ω, α = 30°)	0.210	0.201
45% (c–a at R_f = 70 Ω, α = 30°)	0.198	0.167
55% (a–b at R_f = 20 Ω, α = 60°)	0.847	0.798
55% (a–b at R_f = 200 Ω, α = 60°)	0.689	0.618
65% (b–c at R_f = 50 Ω, α = 30°)	0.755	0.742
90% (ab–g at R_f = 20 Ω, α = 45°)	0.701	0.682
90% (abc at R_f = 50 Ω, α = 60°)	0.694	0.657
90% (abc–g at R_f = 20 Ω, α = 90°)	0.706	0.699
90% (abc–g at R_f = 200 Ω, α = 90°)	0.695	0.628

3.2 FLS for fault section identification

After feature extraction using a wavelet transform, the automatic fault section identifier is designed using an FLS [12]. Fuzzy logic is highly suitable for handling uncertainties such as a fault process that is subject to wide variations in operating conditions of the power system network. The FLS is designed using the information of different types of fault conditions. Then, a fuzzy IF-THEN rule base is formulated for fault section identification. The FLS is designed as follows. For an 'M' class classification with 'n' feature vectors, the rule is L_j: If x_1 is $\boldsymbol{P}_{j1}$ and x_n is $\boldsymbol{P}_{jn}$, then the class is $\boldsymbol{M}_j$, where $\boldsymbol{j} = 1, 2, 3 \ldots \boldsymbol{N}$ and $\boldsymbol{X} = (\boldsymbol{x}_1, \boldsymbol{x}_2, \ldots, \boldsymbol{x}_n)$. Here, $\boldsymbol{P}_{ji}$ is the linguistic value, 'M' is the respective class and 'N' is the fuzzy IF-THEN rules. The gradation of the rule $\boldsymbol{L}_j$ is found out by the following operation

$$\mu_j(x) = \min\{\mu_{j1(x1)}, \mu_{j2}(x_2), \ldots, \mu_{jn}(x_n)\} \tag{1}$$

doi: 10.1049/iet-gtd:20080285

where $\mu_{ji}(x_i)$ is the membership function of the linguistic value P_{ji}. Now, without a certainty grade [13], the respective pattern can be classified by the single winner rule L_{j+}, defined as

$$\mu_{j+}(x) = \max\{\mu_j(x), j = 1, 2, 3, \ldots, N\} \quad (2)$$

The features x_1 and x_2 are fuzzified with a triangular membership function. The triangular membership function for x_1 is shown in Fig. 3, where the input is partitioned into three classes, low (L), medium (M) and high (H). Similar membership is defined for x_2. The fuzzified inputs are fed to a fuzzy rule base consisting of nine rules.

Fuzzy rule base:

Rule1: If $x_1 = \text{L}$ and $x_2 = \text{L}$, then the fault occurs before the UPFC

Rule2: If $x_1 = \text{L}$ and $x_2 = \text{M}$, then the fault occurs before the UPFC

Rule3: If $x_1 = \text{L}$ and $x_2 = \text{H}$, then the fault occurs before the UPFC

Rule4: If $x_1 = \text{M}$ and $x_2 = \text{L}$, then the fault occurs before the UPFC

Rule5: If $x_1 = \text{M}$ and $x_2 = \text{M}$, then the fault occurs after the UPFC

Rule6: If $x_1 = \text{M}$ and $x_2 = \text{H}$, then the fault occurs after the UPFC

Rule7: If $x_1 = \text{H}$ and $x_2 = \text{L}$, then the fault occurs before the UPFC

Rule8: If $x_1 = \text{H}$ and $x_2 = \text{M}$, then the fault occurs after the UPFC

Rule9: If $x_1 = \text{H}$ and $x_2 = \text{H}$, then the fault occurs after the UPFC

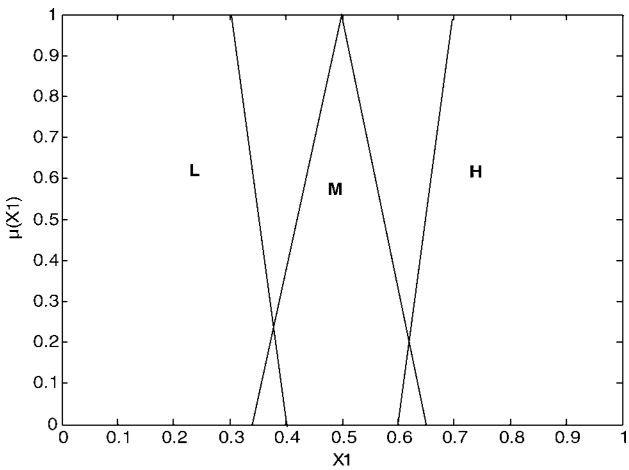

Figure 3 *Triangular membership function*

The results obtained from the FLS are given in Table 2. When the fuzzified inputs are fed to the fuzzy expert system, one of the above nine rules is fired for each input set, and the corresponding output is '1' for the fault after the UPFC and

Table 2 FLS output for identification of fault section

Fault at different location	FLS output (wavelet)	FLS output (DFT)
a–g ($R_f = 20\ \Omega$, $\alpha = 30^\circ$ at 20%)	0	0
b–g ($R_f = 100\ \Omega$, $\alpha = 45^\circ$ at 20%)	0	0
ab–g ($R_f = 30\ \Omega$, $\alpha = 60^\circ$ at 30%)	0	0
ab ($R_f = 50\ \Omega$, $\alpha = 90^\circ$ at 45%)	0	0
ab ($R_f = 100\ \Omega$, $\alpha = 45^\circ$ at 45%)	0	0
abc ($R_f = 50\ \Omega$, $\alpha = 60^\circ$ at 45%)	0	0
abc–g ($R_f = 50\ \Omega$, $\alpha = 90^\circ$ at 45%)	0	0
abc–g ($R_f = 200\ \Omega$, $\alpha = 90^\circ$ at 45%)	0	0
a–g ($R_f = 20\ \Omega$, $\alpha = 45^\circ$ at 55%)	1	1
ab ($R_f = 50\ \Omega$, $\alpha = 60^\circ$ at 60%)	1	1
ab ($R_f = 200\ \Omega$, $\alpha = 90^\circ$ at 60%)	1	0
bc ($R_f = 120\ \Omega$, $\alpha = 45^\circ$ at 65%)	1	0
ab–g ($R_f = 100\ \Omega$, $\alpha = 30^\circ$ at 65%)	1	0
abc ($R_f = 150\ \Omega$, $\alpha = 60^\circ$ at 70%)	1	0
abcg ($R_f = 150\ \Omega$, $\alpha = 90^\circ$ at 85%) with source impedance changed (increased by 10%)	1	0
abcg ($R_f = 150\ \Omega$, $\alpha = 60^\circ$ at 85%) with source impedance changed (increased by 30%)	1	0
abcg ($R_f = 200\ \Omega$, $\alpha = 90^\circ$ at 90%) with source impedance changed (increased by 30%)	1	0

doi: 10.1049/iet-gtd:20080285

'0' for a fault before the UPFC. For an 'a–g' fault with fault resistance $R_f = 20\ \Omega$, inception angle $\alpha = 30^\circ$ at 20% of the line, the FLS provides '0' as the output. This shows that the fault occurred before the UPFC (not including the UPFC). However, for a similar fault with fault resistance $R_f = 20\ \Omega$, inception angle $\alpha = 45^\circ$ at 55% of the line, the output is '1', which means that the fault occurred after the UPFC (including the UPFC). The proposed FLS has been tested for fault situations with $R_f = 200\ \Omega$ and inception angle $\alpha = 90^\circ$, which are the extreme cases, and it provides accurate results. Similar results are computed using the Discrete Fourier Transform (DFT) and FLS for fault section identification and the results of comparison between the proposed wavelet transform and FLS, are depicted in Table 2. In the comparison, it is found that the DFT is unable to identify the fault section for remote-end faults and faults with high fault resistance.

4 Fault location determination using differential equation approach

After the fault section is identified, the control shifts to the differential equation-based fault locator. The fault location is determined in terms of the line inductance to the fault location from the relaying point. The line inductance is determined using a differential equation approach separately for faults before and after the UPFC using synchronised current and voltage signals of both the sending and receiving ends. The control shifts to the appropriate differential equation-based algorithm depending upon the fault section. The following section deals with the determination of the fault location for faults occurring before and after the UPFC using a differential equation approach.

4.1 Pre-fault parameter setting

Initially, the pre-fault condition of the UPFC-based line is studied according to the model given in Fig. 1*a*. The power flow equations are formulated and solved using the Newton-Raphson method. The phase angles and voltage magnitudes of all the buses are found out at a constant shunt voltage, which are as follows

Series injected voltage-	Ese (pu)
Series current-	Ise (pu)
Series injected voltage phase angle-	Thse (radian)
Shunt voltage-	Esh (pu)
Shunt current-	Ish (pu)
Voltage of the UPFC bus-	Vupfc (pu)
Phase angle of the UPFC bus-	Thupfc (radian)

Thus, the series injected voltage and phase angle result for specific operating pre-fault conditions. The different shunt voltages 'Esh' at which the parameters of the different buses are found out are 1.0 pu (per unit), 1.05 and 0.95 pu. Table 3 shows the different magnitudes and phase angles at Esh = 1.0 pu. The above study was made with different loading conditions of P_L and Q_L. After obtaining the different values of series injected voltage and phase angle for the pre-fault condition, the parameters of the UPFC model developed using PSCAD are set and faults are created with various operating conditions like variations in fault resistance, inception angle and fault locations. The magnitude and phase angle of the series injected voltage plays a vital role in the functionality of the UPFC.

4.2 Current injection-based UPFC model

The UPFC consists of shunt and series voltages with the respective impedances as shown in Fig. 1*a*. However, the proposed technique uses the current injection model for the determination of fault location in terms of the line inductance. The original model is reduced to the current injection model, and the equivalent impedance models are shown in Figs. 4*a* and 4*b*, respectively.

4.3 Differential equation-based fault locator

4.3.1 Fault locator for fault at F1(before UPFC):

For a fault at F1($\times$ from the relaying point), before the UPFC, the UPFC-based line and the equivalent model are developed and are shown in Figs. 5*a* and 5*b*, respectively. R, L and C are the line parameters, Y_F is the fault path

Table 3 Power flow solutions for pre-fault situation with Esh = 1.0 pu

Ish	Ise	Ese	Thse	Vupfc	Thupfc	(P_L Q_L)
0.4475	0.2854	0.1087	0.9714	0.9910	0.0301	(0.2 0.2)
0.4475	0.3636	0.1197	1.0244	0.9916	0.0276	(0.3 0.2)
0.4475	0.5026	0.1371	0.9864	0.9948	0.0252	(0.4 0.3)
0.4475	0.5861	0.1480	1.0321	0.9949	0.0226	(0.5 0.3)
0.4475	0.7063	0.1615	0.8878	1.0011	0.0234	(0.5 0.5)
0.4475	0.9425	0.1929	1.0134	1.0010	0.0154	(0.8 0.5)
0.4475	0.7226	0.1652	1.0012	0.9980	0.0202	(0.6 0.4)

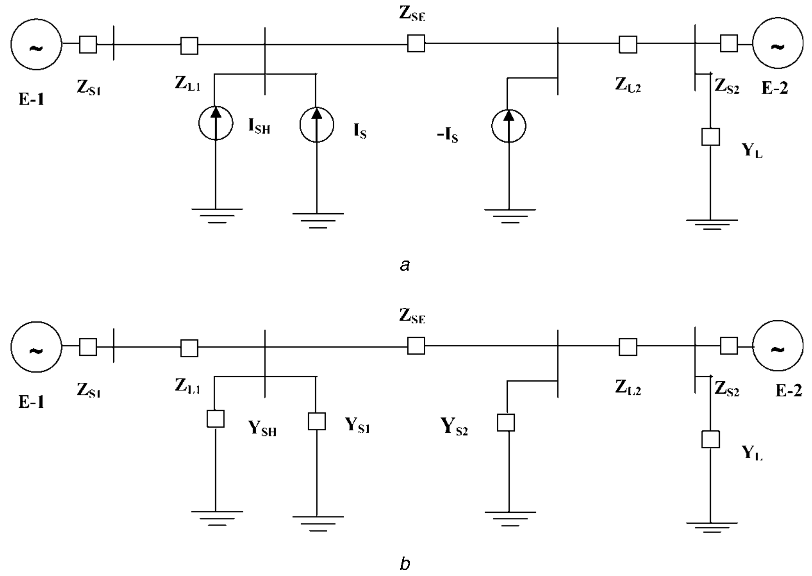

Figure 4 *Equivalent current injection and admittance model*

a Equivalent current injection model
b Equivalent admittance model

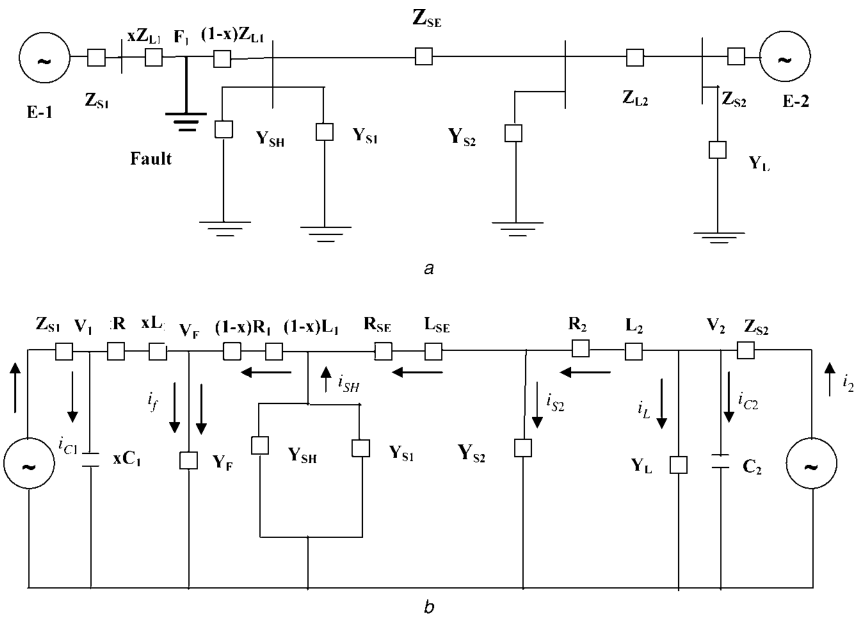

Figure 5 *UPFC-based line and equivalent model for fault at F1*

a UPFC-based line for fault at F1
b Equivalent model for Fault at F1

admittance; and 'v' and 'i' are the voltage and current at the sending and receiving ends. If the fault occurs at F1, then the voltage equation around the fault point F1 is given as

$$xR_1(i_1 - i_{c1}) + xL_1 \frac{\mathrm{d}}{\mathrm{d}t}(i_1 - i_{c1}) + v_f = v_1$$

$$\Rightarrow xR_1 i_1 - x^2 R_1 C_1 \frac{\mathrm{d}v_1}{\mathrm{d}t} + xL_1 \frac{\mathrm{d}i_1}{\mathrm{d}t} - x^2 L_1 C_1 \frac{\mathrm{d}^2 v_1}{\mathrm{d}t^2} + \frac{i_\mathrm{f}}{Y_\mathrm{F}} = v_1 \tag{3}$$

The corresponding fault current i_f can be derived as

$$\begin{aligned} i_\mathrm{f} &= (i_1 - i_{c1}) + (i_2 - i_{c2} - i_L - i_{s2} + i_{SH}) \\ &= \left(i_1 - xC_1 \frac{\mathrm{d}v_1}{\mathrm{d}t}\right) + \left(i_2 - C_2 \frac{\mathrm{d}v_2}{\mathrm{d}t} - v_2 Y_L \right. \\ &\quad \left. - Y_{s2}\left[v_2 - R_2(i_2 - i_{c2} - i_L) - L_2 \frac{\mathrm{d}}{\mathrm{d}t}(i_2 - i_{c2} - i_L)\right]\right. \end{aligned}$$

doi: 10.1049/iet-gtd:20080285

$$+(Y_{SH}+Y_{SI})\left[\begin{array}{c} v_2 - R_2(i_2 - i_{c2} - i_L) \\ -L_2\dfrac{\mathrm{d}}{\mathrm{d}t}(i_2 - i_{c2} - i_L) \\ -R_{\mathrm{SE}}(i_2 - i_{c2} - i_L - i_{s2}) \\ -L_{\mathrm{SE}}\dfrac{\mathrm{d}}{\mathrm{d}t}(i_2 - i_{c2} - i_L - i_{s2}) \end{array}\right]\Bigg) \tag{4}$$

Putting the value i_f in (3) and expanding further results in

$$\begin{aligned}
&\left(xR_1+\frac{1}{Y_F}\right)i_1+xL_1\frac{\mathrm{d}_i}{\mathrm{d}t}-\left(x^2R_1C_1+\frac{C_1}{Y_F}\right)\frac{\mathrm{d}v_1}{\mathrm{d}t} \\
&-x^2L_1C_1\frac{\mathrm{d}^2v_1}{\mathrm{d}t^2} \\
&+\left[\begin{array}{c}\dfrac{1}{Y_{\mathrm{F}}}+\dfrac{Y_{S2}}{Y_F}-\dfrac{(Y_{SH}+Y_{S1})R_2}{Y_{\mathrm{F}}}-\dfrac{(Y_{SH}+Y_{S1})R_{SE}}{Y_{\mathrm{F}}} \\ +\dfrac{(Y_{SH}+Y_{S1})Y_{S2}R_2R_{SE}}{Y_{\mathrm{F}}}\end{array}\right]i_2 \\
&+\left[\frac{(Y_{S2}L_2)}{Y_{\mathrm{F}}}-\frac{(Y_{SH}+Y_{S1})_2}{Y_{\mathrm{F}}}-\frac{(Y_{SH}+Y_{S1})Y_{S2}L_2R_{SE}}{Y_{\mathrm{F}}}\right. \\
&\left.-\frac{(Y_{SH}+Y_{S1})L_SY_{S2}R_2}{Y_{\mathrm{F}}}\right]\frac{\mathrm{d}i_2}{\mathrm{d}t}-\left[\frac{(Y_{SH}+Y_S)}{Y_{\mathrm{F}}}L_{SE}Y_{S2}L_2\right]\frac{\mathrm{d}^2i_2}{\mathrm{d}t^2} \\
&+\left[\frac{(Y_{S1}R_2Y_L)}{Y_{\mathrm{F}}}+\frac{(Y_{SH}+Y_{S1})}{Y_{\mathrm{F}}}+\frac{(Y_{SH}+Y_{S1})R_2Y_L}{Y_{\mathrm{F}}}+\frac{Y_L}{Y_{\mathrm{F}}}\right. \\
&+\frac{(Y_{SH}+Y_{S1})R_{SE}Y_L}{Y_{\mathrm{F}}}+\frac{(Y_{SH}+Y_{S1})R_{SE}Y_{S2}}{Y_{\mathrm{F}}} \\
&\left.-\frac{(Y_{SH}+Y_{S1})R_{SE}Y_{S2}R_2Y_L}{Y_{\mathrm{F}}}\right]v_2 \\
&+\left[\begin{array}{c}\dfrac{C_2}{Y_{\mathrm{F}}}+\dfrac{(Y_{S2}R_2)}{Y_{\mathrm{F}}}+\dfrac{(Y_{S2}Y_LL_2)}{Y_{\mathrm{F}}}+\dfrac{(Y_{SH}+Y_{S1})R_2C_2}{Y_{\mathrm{F}}} \\ +\dfrac{(Y_{SH}+Y_{S1})R_{SE}C_2}{Y_{\mathrm{F}}}-\dfrac{(Y_{SH}+Y_{S1})Y_{S1}C_2R_{SE}}{Y_{\mathrm{F}}} \\ -\dfrac{(Y_{SH}+Y_{S1})R_{SE}Y_{S2}Y_LL_2}{Y_{\mathrm{F}}} \\ -\dfrac{(Y_{SH}+Y_{S1})Y_{S2}R_2C_2R_{SE}}{Y_{\mathrm{F}}} \\ -\dfrac{(Y_{SH}+Y_{S1})R_{SE}Y_{S2}R_2Y_LL_2}{Y_{\mathrm{F}}} \\ +\dfrac{(Y_{SH}+Y_{S1})R_{SE}Y_{S2}R_2C_2}{Y_{\mathrm{F}}}- \\ \dfrac{(Y_{SH}+Y_{S1})L_{SE}Y_{S2}R_2Y_L}{Y_{\mathrm{F}}}\end{array}\right]\frac{\mathrm{d}v_2}{\mathrm{d}t} \\
&+\left[\frac{(Y_{SH}+Y_{S1})Y_{S2}L_2C_2}{Y_{\mathrm{F}}}+\frac{(Y_{SH}+Y_{S1})Y_{S2}L_2C_2R_{SE}}{Y_{\mathrm{F}}}\right. \\
&\left.+\frac{(Y_{SH}+Y_{S1})L_{SE}Y_{S2}C_2R_2}{Y_{\mathrm{F}}}+\frac{(Y_{SH}+Y_{S1})L_{SE}Y_{S2}Y_LL_2}{Y_{\mathrm{F}}}\right]\frac{\mathrm{d}^2v_2}{\mathrm{d}t^2} \\
&+\left[\frac{(Y_{SH}+Y_{S1})L_{SE}Y_{S2}L_2C_2}{Y_{\mathrm{F}}}\right]\frac{\mathrm{d}^3v_3}{\mathrm{d}t^3}=v_1
\end{aligned} \tag{5}$$

The differential equation (5) can be represented as a difference equation and in a matrix form as below

$$\left[\begin{array}{cc|cccc} m_{11} & m_{12} & m_{13} & m_{14} & \cdots & m_{111} \\ m_{21} & m_{22} & m_{23} & m_{24} & \cdots & m_{211} \\ \hline m_{31} & m_{32} & m_{33} & m_{43} & \cdots & m_{311} \\ \vdots & & & & & \\ m_{111} & m_{112} & m_{113} & m_{114} & \cdots & m_{1111} \end{array}\right]\left[\begin{array}{c} n_1 \\ n_2 \\ \hline n_3 \\ \vdots \\ n_{11} \end{array}\right]=\left[\begin{array}{c} o_1 \\ o_2 \\ \hline o_3 \\ \vdots \\ o_{11} \end{array}\right] \tag{6}$$

where

$$m_{N1}=\frac{\Delta t}{2}(i_{1k+N}+i_{1k+N-1}),\quad m_{N2}=(i_{1k+N}-i_{1k+N-1}),$$
$$m_{N3}=-(v_{1k+N}-v_{1k+N-1})$$
$$m_{N4}=-\frac{1}{\Delta t}(v_{1k+N}-2v_{1k+N-1}+v_{1k+N-2}),$$
$$m_{N5}=\frac{\Delta t}{2}(i_{2k+N}+i_{1k+N-1}),\quad m_{N6}=(i_{2k+N}-i_{2k+N-1})$$
$$m_{N7}=-\frac{1}{\Delta t}(i_{2k+N}-2i_{2k+N-1}+i_{1k+N-2}),$$
$$m_{N8}=\frac{\Delta t}{2}(v_{2k+N}+v_{2k+N-1}),\quad m_{N9}=(v_{2k+N}+v_{21k+N-1})$$
$$m_{N10}=\frac{1}{\Delta t}(v_{2k+N}-2v_{2k+N-1}+v_{21k+N-1}),$$
$$m_{N11}=\frac{1}{\Delta t^2}(v_{2k+N}-3v_{2k+N-1}+3v_{2k+N-2}-v_{21k+N-1})$$
$$O_N=\frac{\Delta t}{2}(v_{1k+N}+v_{1k+N-1})$$

$i_{1k}, i_{1k+1}, \ldots, i_{1k+11}$ samples of i_1

$i_{2k}, i_{2k+1}, \ldots, i_{2k+11}$ samples of i_2

$v_{1k}, v_{1k+1}, \ldots, v_{1k+11}$ samples of v_1

$v_{2k}, v_{2k+1}, \ldots, v_{2k+11}$ samples of v_2

k is the sample number and Δt the sampling interval

The divided parts of the (6) can be represented as

$$\left[\begin{array}{c|c} G_1 & G_2 \\ \hline G_3 & G_4 \end{array}\right]\left[\begin{array}{c} H_1 \\ \hline H_2 \end{array}\right]=\left[\begin{array}{c} Y_1 \\ \hline Y_2 \end{array}\right] \tag{7}$$

where

$$H_1 = \begin{bmatrix} n_1 \\ n_2 \end{bmatrix} = [G_1 - G_2 G_4^{-1} G_3]^{-1} [Y_1 - G_2 G_4^{-1} Y_2] \quad (8)$$

$$n_2 = xL_1$$

n_1 and n_2 are found out from (8), and $n_2 = xL_1$ is the desired estimate of the line inductance to the fault point from the relaying end. As the line inductance is directly proportional to the fault location from the relaying point, the fault location is found out accurately.

4.3.2 Fault locator for fault at F2 (After UPFC):

For a fault at F2 (x from the receiving end), after the UPFC, the UPFC-based line and the equivalent model are developed and shown in Fig. 6a and 6b, respectively. R, L and C are the line parameters; Y_F is the fault path admittance; and 'v' and 'i' are the voltage and current at the sending and receiving ends. If the fault occurs at F2, then the voltage equation around the fault point F2 is given as

$$\begin{aligned} &xR_2(i_2 - i_{c2} - i_L) + xL_2 \frac{\mathrm{d}}{\mathrm{d}t}(i_2 - i_{c2} - i_L) + v_f = v_2 \\ &\Rightarrow xR_2\left(i_2 - xC_2\frac{\mathrm{d}v_2}{\mathrm{d}t} - v_2 Y_L\right) + xL_2 \frac{\mathrm{d}}{\mathrm{d}t} \\ &\times \left(i_2 - xC_2\frac{\mathrm{d}v_2}{\mathrm{d}t} - v_2 Y_L\right) + v_f = v_2 \end{aligned} \quad (9)$$

The fault current i_f is derived as

$$\begin{aligned} i_f &= (i_1 - i_{c1} + i_{SH} - I_{S2}) + (i_2 - i_{c2} - i_L) \\ &= \left(i - 1 - C_1\frac{\mathrm{d}v_1}{\mathrm{d}t}\right) + (Y_{S1} + Y_{SH})v_1 - i_{SE} \\ &\quad + \left(i_2 - xC_2\frac{\mathrm{d}v_2}{\mathrm{d}t} - v_2 Y_L\right) \end{aligned} \quad (10)$$

Now, putting the value of i_f in (9) and expanding further results in

$$\begin{aligned} &\left[\frac{1}{Y_F} + \frac{Y_{S2}R_1}{Y_F} + \frac{Y_{S2}R_{SE}}{Y_F} - \frac{Y_{S2}(Y_{SH}+Y_{S1})R_{SE}R_1}{Y_F}\right] i_1 \\ &+ \begin{bmatrix} -\frac{(Y_{SH}+Y_{S1})L_1}{Y_F} - \frac{(Y_{SH}+Y_{S1})Y_{S2}L_1R_{SE}}{Y_F} - \\ +\frac{L_1Y_{S2}}{Y_F} + \frac{L_{SE}Y_{S2}}{Y_F} \\ \frac{(Y_{SH}+Y_{S1})Y_{S2}L_{SE}R_1}{Y_F} \end{bmatrix} \frac{\mathrm{d}i_2}{\mathrm{d}t} \\ &- \left[\frac{(Y_{SH}+Y_{S1})Y_{S2}L_{SE}L_1}{Y_F}\right] \frac{\mathrm{d}^2 i_1}{\mathrm{d}t^2} \\ &+ \left[\frac{(Y_{SH}+Y_{S1})+Y_{S2}+Y_{SE}(Y_{S1}+Y_{SH})R_{SE}}{Y_F}\right] v_1 \\ &+ \begin{bmatrix} \frac{C_1}{Y_F} - \frac{(Y_{S1}+Y_{SH})R_1C_1}{Y_F} + \frac{Y_{S2}R_1C_1}{Y_F} - \frac{Y_{S2}L_1C_1}{Y_F} \\ + \frac{Y_{S2}C_1R_{SE}R_1(Y_{SH}+Y_1)}{Y_F} + \frac{Y_{S2}L_{SE1}(Y_{SH}+Y_1)}{Y_F} \end{bmatrix} \frac{\mathrm{d}v_1}{\mathrm{d}t} \\ &- \left[-\frac{L_1C_1(Y_{SH}+Y_1)}{y_F} + \frac{Y_{S2}R_{SE}L_1C_1(Y_{SH}+Y_1)}{Y_F}\right. \\ &\left. -\frac{Y_{S2}L_{SE}C_1}{Y_F} + \frac{Y_{S2}L_S(Y_{SH}+Y_1)}{Y_F}\right] \frac{\mathrm{d}^2 v_1}{\mathrm{d}t^2} \\ &+ \frac{Y_{S1}L_{SE}L_1C_1}{Y_F}\frac{\mathrm{d}^3 v_1}{\mathrm{d}t^3} + \frac{xR_2}{Y_F} i_2 + xL_2\frac{\mathrm{d}i_2}{\mathrm{d}t} \\ &- \left[\frac{Y_L}{Y_F} + xR_2Y_L\right] v_2 - \left[\frac{xC_2}{Y_F} + x^2R_2C_2 + xY_LL_2\right]\frac{\mathrm{d}v_2}{\mathrm{d}t} \\ &- x^2L_2C_2\frac{\mathrm{d}^2 v_2}{\mathrm{d}t^2} = v_2 \end{aligned} \quad (11)$$

The differential equation (11) can be represented as a difference equation and in a matrix form as below

$$\left[\begin{array}{cc|ccc} m_{11} & m_{12} & m_{13} & m_{14} \cdots & m_{112} \\ m_{21} & m_{22} & m_{23} & m_{24} \cdots & m_{212} \\ \hline m_{31} & m_{32} & m_{33} & m_{43} \cdots & m_{312} \\ \vdots & & & & \\ m_{121} & m_{122} & m_{123} & m_{124} \cdots & m_{1212} \end{array}\right] \left[\begin{array}{c} n_1 \\ n_2 \\ \hline n_3 \\ \vdots \\ n_{12} \end{array}\right] = \left[\begin{array}{c} o_1 \\ o_2 \\ \hline o_3 \\ \vdots \\ o_{12} \end{array}\right] \quad (12)$$

where

$$m_{N1} = \frac{\Delta t}{2}(i_{2k+N} + i_{2k+N-1}),\ m_{N2} = (i_{2k+N} - i_{2k+N-1})$$

$$m_{N3} = -\frac{\Delta t}{2}(v_{2k+N} + v_{2k+N-1}),\ m_{N4} = -(v_{2k+N} - v_{2k+N-1})$$

$$m_{N5} = -\frac{1}{\Delta t}(v_{2k+N} - 2v_{2k+N-1} + v_{2k+N-2})$$

$$m_{N6} = \frac{\Delta t}{2}(i_{1k+N} - i_{1k+N-1}),\ m_{N7} = (i_{1k+N} - i_{1k+N-1})$$

$$m_{N8} = -\frac{1}{\Delta t}(i_{1k+N} - 2i_{1k+N-1} + i_{1k+N-2})$$

$$m_{N9} = -\frac{\Delta t}{2}(v_{1k+N} + v_{1k+N-1})$$

doi: 10.1049/iet-gtd:20080285

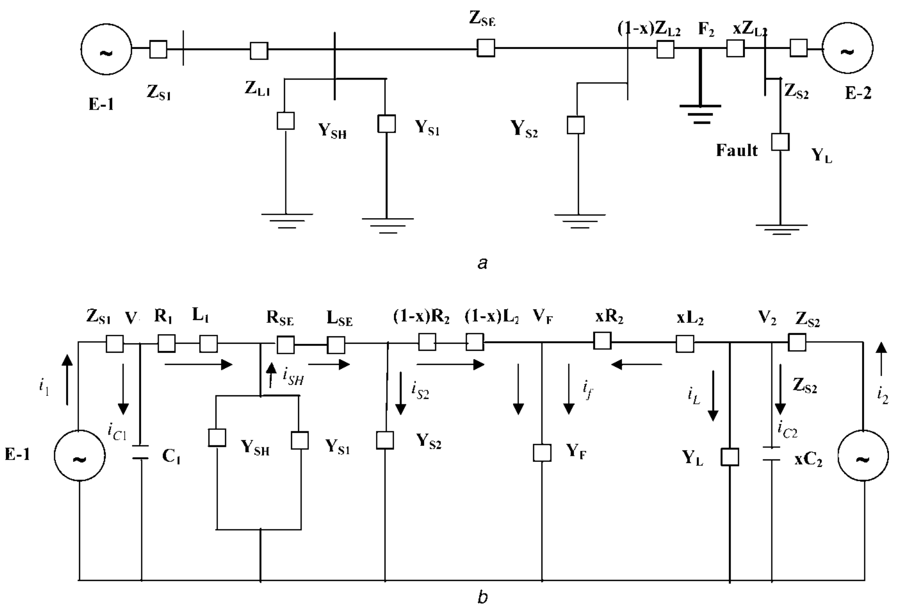

Figure 6 *UPFC-based line and equivalent model for fault at F2*

a UPFC-based line for fault at F2

b Equivalent model for fault at F2

$$m_{N10} = (v_{1k+N} - v_{1k+N-1})$$

$$m_{N11} = -\frac{1}{\Delta t}(v_{1k+N} - 2v_{1k+N-1} + v_{1k+N-1})$$

$$m_{N12} = \frac{1}{\Delta t^2}(v_{1k+N} - 3v_{1k+N-1} + 3v_{1k+N-2} - v_{1k+N-3})$$

$$O_N = \frac{\Delta t}{2}(v_{1k+N} + v_{1k+N-1})$$

$i_{1k}, i_{1k+1}, \ldots, i_{1k+12}$ samples of i_1

$i_{2k}, i_{2k+1}, \ldots, i_{1k+12}$ samples of i_2

$v_{1k}, v_{1k+1}, \ldots, v_{1k+12}$ samples of v_1

$v_{2k}, v_{2k+1}, \ldots, v_{2k+12}$ samples of v_2

k is the sample number and Δt the sampling interval

The divided parts of the equation (12) can be represented as

$$\left[\begin{array}{c|c} G_1 & G_2 \\ \hline G_3 & G_4 \end{array}\right]\left[\begin{array}{c} H_1 \\ \hline H_2 \end{array}\right] = \left[\begin{array}{c} Y_1 \\ \hline Y_2 \end{array}\right] \quad (13)$$

$$H_1 = \begin{bmatrix} n_1 \\ n_2 \end{bmatrix} = [G_1 - G_2 G_4^{-1} G_3]^{-1}[Y_1 - G_2 G_4^{-1} Y_2] \quad (14)$$

$$n_2 = xL_2$$

n_1 and n_2 are found out from the (14), and n_2 is the desired estimate of the line inductance to the fault point. Here, 'xL_2' is the line inductance of the fault point from the receiving end. Thus, fault location from the relaying point is found out by deducting 'xL_2' from the line inductance of the complete line.

4.4 Computational results for fault location

The fault location is determined in terms of the inductance to the fault point. For a fault at 'F1' (before the UPFC), the line inductance measured is 'xL_1' from the relaying point. Similarly, 'xL_2' measured from the receiving end, provides the fault location from the receiving end for a fault at 'F2'. The fault location for a fault at 'F2' from the relaying point is found out by deducting 'xL_2' from the line inductance of the complete transmission line. The error in fault location is calculated as follows

$$\%\ \text{error} = \frac{xL_e - xL}{L} \times 100 \quad (15)$$

where xL_e is the estimated line inductance to the fault point and xL the actual line inductance to the fault point. 'L' represents the line inductance of the transmission line for its complete length.

Tables 4–9 depict the fault location for different operating conditions of the line and the UPFC. The series injected voltage phase angle 'Thse' resultant from the power flow solution is in radian and converted to degree before setting the value in the UPFC model. The inception angle of the fault is represented by 'α'. Table 4 provides the fault location for an 'L–G' (a–g) fault with 'Ese' = 0.1371 and

doi: 10.1049/iet-gtd:20080285

Table 4 Fault location for 'a–g' fault at 10% of line with different fault resistance at Esh = 1.0 pu

Fault resistance, Ω	$\alpha = 30°$, 10% of line, L–G fault	
	$xL_1 = 40.5$ mH	
	xLe_1	Error, %
$R_F = 0$	41.05	0.13
$R_F = 30$	43.58	0.76
$R_F = 70$	45.48	1.22
$R_F = 100$	48.96	2.08
$R_F = 120$	51.25	2.65
$R_F = 150$	52.69	3.00
$R_F = 170$	54.21	3.38
$R_F = 200$	56.98	4.06

Ish = 0.4475; Ise = 0.5026; Ese = 0.1371; Thse = 0.9864; Vupfc = 0.9948; Thupfc = 0.0252; $P_L = 0.4$; $Q_L = 0.3$

'Thse' = 0.9864 (28.25°) at 10% of the line. The error in fault location is 0.13% when $R_F = 0\,\Omega$. However, the location error increases to 4.06% for $R_F = 200\,\Omega$ for a similar fault situation. Table 5 shows the fault location for an 'LL–G' (ab–g) fault with 'Ese' = 0.1480 and 'Thse' = 1.0321 (29.56°) at 45% of the line. The errors are 0.05% and 3.85% for R_F of 0 and 200 Ω, respectively. Table 6 depicts the fault location for an 'L–G' (b–g) fault with 'Ese' = 0.1676 and 'Thse' = 0.9754 (27.94°) at 90% of the line. Here, the inductance xL_2 is measured from the other end (receiving end), and the corresponding line inductance from the relaying point (xL_1) is found out by deducting it from the total line inductance. The error varies

Table 5 Fault location for 'ab–g' fault at 45% of line with different fault resistance at Esh = 1.0 pu

Fault resistance, Ω	$\alpha = 40°$, 45% of line, L–G fault	
	$xL_1 = 182.25$ mH	
	xLe_1	Error, %
$R_F = 0$	182.49	0.05
$R_F = 30$	183.45	0.29
$R_F = 70$	187.59	1.31
$R_F = 100$	189.25	1.72
$R_F = 120$	190.85	2.12
$R_F = 150$	192.38	2.50
$R_F = 170$	195.69	3.31
$R_F = 200$	197.85	3.85

Ish = 0.4475; Ise = 0.5861; Ese = 0.1480; Thse = 1.0321; Vupfc = 0.9949; Thupfc = 0.0226; $P_L = 0.5$; $Q_L = 0.3$

Table 6 Fault location for 'b–g' fault at 90% of line with different fault resistance at Esh = 1.05 pu

Fault resistance, Ω	$\alpha = 90°$, 90% of line, L–G fault	
	$xL_2 = 40.5$ mH ($xL_1 = 364.5$ mH)	
	xLe_1	Error, %
$R_F = 0$	366.98	0.61
$R_F = 30$	369.85	1.32
$R_F = 70$	372.45	1.96
$R_F = 100$	376.54	2.97
$R_F = 120$	379.58	3.72
$R_F = 150$	381.45	4.18
$R_F = 170$	384.59	4.96
$R_F = 200$	386.98	5.55

Ish = 0.9475; Ise = 0.7189; Ese = 0.1676; Thse = 0.9754; Vupfc = 1.0058; Thupfc = 0.0152; $P_L = 0.8$; $Q_L = 0.5$

Table 7 Fault location for b–g fault at 15% of line with different series injected voltage Esh = 1.0 pu, $P_L = 0.6$ pu and $Q_L = 0.4$ pu

Series injected voltage Ese in %	$\alpha = 30°$, 15% line, L–G fault			
	$xL_1 = 60.75$ mH			
	$R_F = 30\,\Omega$		$R_F = 150\,\Omega$	
	xLe_1	Error, %	xLe_1	Error, %
0	62.69	0.47	64.56	0.94
2	64.59	0.94	67.85	1.75
5	66.87	1.51	69.84	2.24
7	69.98	2.27	72.45	2.88
10	72.45	2.88	75.48	3.63
12	75.85	3.72	78.98	4.50
15	78.45	4.37	81.95	5.23

Ish = 0.4475; Ise = 0.7226; Thse = 1.0012; Vupfc = 0.9980; Thupfc = 0.0202; $P_L = 0.6$; $Q_L = 0.7$

IET Gener. Transm. Distrib., 2009, Vol. 3, No. 1, pp. 86–98
doi: 10.1049/iet-gtd:20080285

Table 8 Fault location for c–g fault at 15% of line with different series injected voltage phase angle at Esh = 1.0 pu, $P_L = 0.5$ pu and $Q_L = 0.5$ pu

Series injected voltage phase angle 'Thse' in degree (series injected voltage at 10%)	$\alpha = 30^\circ$, 25% of line, L–G fault			
	xL_1 =101.25 mH			
	$R_F = 30\ \Omega$		$R_F = 150\ \Omega$	
	xLe_1	Error, %	xLe_1	Error, %
0	104.52	0.80	106.54	1.30
45	107.58	1.56	1.09.68	2.08
90	109.56	2.05	110.25	2.22
135	112.87	2.86	113.65	3.06
180	116.54	3.77	115.68	3.56
270	119.84	4.59	119.85	4.59
360	123.45	5.48	124.56	5.75

Ish = 0.4475; Ise = 0.7063; Ese = 0.1615; Vupfc = 1.0011; Thupfc = 0.0234; $P_L = 0.5$; $Q_L = 0.5$

from 0.61 to 5.55% for variation in the fault resistance from 0 to 200 Ω, respectively. Table 7 depicts the fault location for an 'L–G' (b–g) fault at 15% of the line with variations in the series injected voltage from 0 to 15% of the line voltage. The error varies from 0.47 to 4.37% when the series injected voltage varies from 0 to 15%, respectively, with a fault resistance of 30 Ω. However, the fault location errors vary from 0.94 to 5.23% with a fault resistance of 150 Ω, with other operating conditions remaining the same.Table 8 provides the fault location for variation in the series injected voltage phase angle with a series injected voltage at 10%. The fault location error varies from 0.80 to 5.48% for a variation of the phase angle from 0° to 360°, respectively, and with fault resistance of 30 Ω. However, the errors vary from 1.30 to 5.75% with a fault resistance of 150 Ω. Table 9 depicts the fault location for different loading conditions with variations in the fault resistance, and the fault location error is restricted below 2%. It is observed that the fault location error increases when the fault impedance, series injected voltage and series injected voltage phase angle increase, which are three important parameters for transmission line fault location process with the UPFC.

Table 9 Fault location for a–g fault at 45% of line with different loading conditions at Esh = 1.0

Loading conditions		$\alpha = 30^\circ$, 45% of line, L–G fault			
		xL_1 =182.25 mH			
		$R_F = 30\ \Omega$		$R_F = 150\ \Omega$	
		xLe_1	Error, %	xLe_1	Error, %
P_L	Q_L	183.96	0.42	184.56	0.57
0.2	0.2	184.56	0.57	186.95	1.16
0.3	0.2	183.89	0.40	185.69	0.84
0.4	0.3	187.54	1.30	188.69	1.59
0.5	0.3	184.96	0.66	188.46	1.53
0.6	0.4	186.95	1.1	186.78	1.11
0.8	0.5	185.78	0.87	187.56	1.31

Ish = 0.4475; Ise = 0.9425; Thse = 1.0134; Ese = 0.1929; Vupfc = 1.0134; Thupfc = 1.0010

The fault location errors from the proposed study have been compared with the existing works, which does not include FACTS, in the transmission line. The wavelet-based approach [14] has a fault location error of up to 4.13%, and the online trained neural network [15] has a location error of up to 3.5%. However, the proposed study has fault location errors within 3–4% for average operating conditions, but it goes up to 5.75% in the case of extreme operating conditions of the UPFC and fault condition in the transmission line. Thus, the proposed technique provides better results with the UPFC compared with the exiting techniques without FACTS units in the transmission line.

The identification of the fault section is achieved within a half cycle (10 ms) from the inception of the fault. Then, the control shifts to the differential equation-based fault locator. As the fault locator takes 12 (maximum) samples for location calculation, the time taken for the fault location is 12 ms. Thus, the total time taken for the identification of the fault section and fault location is 22 ms from the inception of the fault on a cycle time of 20 ms. As the proposed scheme works under the assumption that the phasors measured at the sending and receiving end are synchronised, the time consumed excludes the time of synchronisation. Synchronisation ensures that the samples from the two ends can be time aligned. Consequently, the effect on the performance of protection from variation in the channel delay [16] can be ignored by proper synchronisation. The synchronised measurement is achieved using the global positioning system [17, 18], which can easily and precisely provide a time signal, with an accuracy of 1 µs, at any location on the power network, satisfying the requirement of system protection.

5 Conclusions

The proposed method finds the fault location in the transmission line in the presence of the UPFC using synchronised phasor measurements. This includes developing a transmission line model employing a UPFC and its control. The fault location is determined in terms of the line inductance measured from the relaying end to the fault point. The first part identifies the fault section using a wavelet-fuzzy discriminator, providing an output '0' for a fault before the UPFC and '1' for a fault after the UPFC.

After the identification of the fault section, the fault location is determined using a differential equation-based approach. The fault location error varies from 0.05% under normal operating conditions to 5.75% under extreme operating conditions (fault resistance of 150 Ω, series injected voltage phase angle of 360° and series injected voltage magnitude of 10%). Thus, the proposed method provides a fast and robust fault locator for a transmission line with a UPFC having wide variations in operating conditions with a pre-fault parameter setting.

6 References

[1] NOROOZIAN M., ANGQUIST L., GHANDHARI M., ANDERSON G.: 'Improving power system dynamics by series connected FACTS devices', *IEEE Trans. Power Deliv.*, 1997, **12**, (4), pp. 1635–1641

[2] GYUGYI L.: 'Unified power flow concept for flexible AC transmission systems', *IEE Proc., C*, 1992, **139**, (4), pp. 323–332

[3] ZHOU X., WANG H., AGGARWAL R.K., BEAUMONT P.: 'Performance of evaluation of a distance relay as applied to a transmission system with UPFC', *IEEE Trans. Power Deliv.*, 2006, **21**, (3), pp. 1137–1147

[4] EI-ARROUDI K., JOOS G., MCGILLS D.T.: 'Operation of impedance relays with the STATCOM', *IEEE Trans. Power Deliv.*, 2002, **17**, (2), pp. 381–387

[5] KHEDERZADEH M., SIDHU T.S.: 'Impact of TCSC on the protection of Transmission lines', *IEEE Trans. Power Deliv.*, 2006, **21**, (1), pp. 80–87

[6] GIRGIS A., SALLAM A.A., EL-DIN A.K.: 'An adaptive protection scheme for advanced series compensated (ASC) transmission lines', *IEEE Trans. Power Deliv.*, 1998, **13**, (1), pp. 414–420

[7] DASH P.K., PRADHAN A.K., PANDA G., LIEW A.C.: 'Adaptive relay setting for flexible AC transmission systems (FACTS)', *IEEE Trans. Power Deliv.*, 2000, **15**, (1), pp. 38–43

[8] MOHANTY R.N., GUPTA P.B.D.: 'An improved method for digital relaying of transmission line', *Electr. Power Compon. Syst.*, 2004, **32**, pp. 1013–1030

[9] MANN B.J., MORRISON I.F.: 'Relaying a three phase transmission line with a digital computer', *IEEE Trans. Power Appar. Syst.*, 1971, **PAS 90**, (2), pp. 742–750

[10] YAUSSEF O.A.S.: 'New algorithms for phase selection based on wavelet transforms', *IEEE Trans. Power Deliv.*, 2002, **17**, pp. 908–914

[11] YAUSSEF O.A.S.: 'Online applications of wavelet transform to power system relaying', *IEEE Trans. Power Deliv.*, 2003, **18**, (4), pp. 1158–1165

[12] FERRERO A., SANGIOVANNI S., ZAPPIT E.: 'A fuzzy set approach to fault-type identification in digital relaying', *IEEE Trans. Power Deliv.*, 1998, **13**, p. 1093

[13] GUILLAUME S.: 'Designing fuzzy inference systems from data: An interpretability review', *IEEE Trans. Fuzzy Syst.*, 2001, **9**, pp. 426–443

[14] CHANDA D., KISHORE N.K., SINHA A.K.: 'A wavelet multi-resolution analysis for location of faults on transmission lines', *Electr. Power Energy Syst.*, 2003, **20**, pp. 59–69

[15] OSMAN A.H., ABEDELAZIM T., MALIK O.P.: 'Transmission line distance relaying using on-line trained neural networks', *IEEE Trans. Power Deliv.*, 2005, **20**, (2), pp. 1257–1264

[16] LI H.Y., SOUTHERN E.P., CROSSLEY P.A., *ET AL.*: 'A new type of Differential feeder protection relay using the global positioning system for data synchronization', *IEEE Trans. Power Deliv.*, 1997, **12**, (3), pp. 1090–1099

[17] PHADKE A.G.: 'Synchronized phasor measurements in power systems', *IEEE Comput. Appl. Power J.*, 1993, **6**, (2), pp. 10–15

[18] Working group H-7: 'Synchronized sampling and phasor measurement for relaying and control', *IEEE Trans. Power Deliv.*, 1994, **9**, (1), pp. 442–452

doi: 10.1049/iet-gtd:20080285